Comparative Electrical Conductivity Studies of Samarium and Niobium Oxides-Doped Biochar/Ferrite Nanocomposites

D. Palariya[1, 2*], M. Pandey[1], P. Joshi[3], J. Maheshwari[1], S. Mehtab[1] and M. G. H. Zaidi[1]

[1]*Department of Chemistry, College of Basic Sciences & Humanities, G. B. Pant University of Agriculture and Technology, Pantnagar, U. S. Nagar, India*
[2]*Department of Applied Sciences, Meerut Institute of Engineering and Technology Meerut, Uttar Pradesh, India*
[3]*Catalytic De-Polymerization Area, Upstream & Wax Rheology Division, CSIR-Indian Institute of Petroleum, Dehradun, India*
[*]Corresponding author: palariyadiksha.17@gmail.com

Received 05/05/2025; accepted 05/10/2025
https://doi.org/10.4152/pea.2027450506

Abstract
There has been a surge in demand of electronic devices that serve better durability under adverse environmental conditions. This study investigated electrical conductivity (σDC) of samarium (BFS) and niobium (BFN) doped Biochar/ferrite-based nanocomposites (NC). NC were synthesized using sol-gel method and characterized through Fourier Transform Infrared and UV-diffuse Reflectance Spectroscopy. Structural properties and thermal stability of developed NC were analyzed through Scanning Electron Microscopy and Thermo Gravimetric Analysis. BFS and BFN-based working electrodes (WE) were fabricated by coating them over stainless-steel current collectors, and their surface morphology and electrical properties were investigated. To compare effects of Sm and Nb doping on σDC of NC, measurements of BFS and BFN were performed at variable voltages, temperatures, baking and humid environments. Results showed that BFN had better σDC (0.83 mS/cm) than from BFS counterparts, maybe due to effective incorporation of Nb ions into NC lattice, which improved charge carrier mobility. Arrhenius curve of BFS and BFN was plotted with activation energy value of 27.64 and 26.36 J/mol^{-1}, respectively. Additionally, BFS-derived WE showed higher stability and durability in humid and baking environments. Results demonstrated that BFN can be used as potential candidates for preparing electrode materials.

Keywords: biochar; DC conductivity; electrode materials; ferrite; Nb_2O_5; Sm_2O_3; working electrodes.

Introduction•

Electrically conducting nanocomposites (NC) of metal oxide ferrite nanoparticles (FNP) doped with functionalized biochar (BC) have drawn growing interest as

• The abbreviations list is in pages 423-24.

electrodes in microelectronics, due to their ability to serve as potential electrically conducting materials under harsh environmental conditions of humidity, temperature and radiations [1]. The development of efficient, sustainable and cost-effective electrode materials is crucial for advancements in energy storage and conversion technologies [1]. NC has emerged as highly promising candidates in this field due to their unique properties, which result from the interaction between their different components. BC, a carbon-rich material produced from biomass, has gained attention for its potential in energy storage applications [2]. Its high surface area, porosity and conductive properties make it an excellent component for NC. FNP, known for their magnetic properties and stability; can enhance electrical conductivity and electrochemical performance of NC when integrated into them [3]. BC/FNP-derived NC like BC/graphene/Fe_3O_4, BC/Fe_xO_y, BC/Fe_3O_4, BC/$MnFe_2O_4$, BC/$CoFe_2O_4$ and BC/$NiFe_2O_4$ have been reported on their application in diverse fields [4-12]. Doping FNP with specific elements can further optimize their properties for targeted applications. Specifically, doping with elements such as Sm and Nb has shown promise in improving electrical and electrochemical characteristics of these materials.

Various Nb_2O_5-based NC have been employed as energy storage materials, batteries, supercapacitors, optoelectronics, visible light photocatalyst for H_2 Production, electrochemical sensors, photoelectrochemical water splitting, solar cells and sensors, dye degradation and detection and capture of heavy metals [13-22].

Sm_2O_3-doped NC like Ag/Sm_2O_3/rGO, PANI/Sm_2O_3, Sm_2O_3/rGO and Sm_2O_3/Co_3O_4/PANI applications have been reported in sensing, photocatalysis, catalytic hydrogenation, nanoelectronics, biomedical, antimicrobial, CO conversion, pesticide adsorption and energy storage fields [23-32]. The effect of various environmental factors like baking, humidity exposure and temperature on conductivity of hBN/MWCNT electrode has been reported, showing significant conductivity values [1]. However, literature search reveals that electrical conductivity of NC from rare earth and transition metal oxide doped-BC/FNP has been much less studied.

This manuscript presents a comparative study on electrical conductivity of BC/FNP NC doped with Sm (BFS) and Nb (BFN). Synthesis, characterization and performance assessment of BFS and BFN were conducted to elucidate their structural and morphological properties and to analyze the effects of doping on their electrical properties. The findings will contribute to the development of thermally stable advanced electrode materials for various electrochemical applications.

Experimental

Materials

BC was derived through pyrolysis of *Parthenium hysterophorus*. Ferrous chloride tetrahydrate and ammonia solution were sourced from Molychem. Ethanol, nitric

and sulfuric acids and N-Methyl-2-Pyrrolidone (NMP) solvents were obtained from Loba Chem. Polyvinylbutyral (PVB) was acquired from Himedia, India. Nb_2O_5 and Sm_2O_3 were purchased from Molychem. Deionized water used in all experiments was produced using a PURE ROUP 30 system.

Development of Nb_2O_5 and Sm_2O_3-doped NC

BFS and BFN were prepared using a wet chemical synthesis method with a probe ultrasonicator. In short, 150 mg FNP were added to a BC suspension, and the mixture was ultrasonicated for 45 min. Afterwards, 100 mg Sm_2O_3 was added into it, followed by 20 min ultrasonication. Resulting mixture was then filtered and dried at room temperature for subsequent use. Nb_2O_5-doped NC was similarly prepared [33].

Fabrication of working electrodes

WE were developed by depositing FNP and BC slurry onto a stainless-steel current collector (2 cm² area), which were meticulously cleaned using diluted acid, acetone and distilled water, followed by drying with hot air, to achieve a smooth, shiny surface. The slurry was prepared by mixing 85 mg NC with 15 mg PVB binder in 1 mL NMP solvent, and subjecting the mixture to ultrasonication at 500 rpm, for 30 min. Approxim. 120 µL of this slurry was then deposited onto the current collector surface to form WE with a thickness of 0.1±0.01 cm. These coated WE were left to dry at room temperature for 24 h, and then vacuum dried at 50±1 °C under 400 mm Hg [34].

Characterization

Fourier Transform Infrared (FTIR) spectra were obtained using a Thermo Nicolet instrument, within a wavenumber range from 4000 to 500 cm^{-1}. Surface morphologies were analyzed via scanning electron microscopy (SEM) on a JEOL JSM 6610 LV at a magnification of 10 kx (1 µm) and an accelerating voltage of 10 kV. Additionally, ultraviolet-diffuse reflectance spectroscopy (UV-DRS) was performed using a Shimadzu UV-2450 UV-VIS spectrophotometer. Thermal stability of as-prepared NC was examined using simultaneous TG-DT-DTG (Thermogravimetry-Differential Thermal-Derivative Thermogravimetry) analyses employing EXSTAR TG/DTA 6300 instrument in static air at a heating rate of 10 °C/min up to 1000 °C, with alumina as reference material. TG data are expressed in terms of TG onset, endset and weight residue (Tgo, Tge and Wr %, respectively).

Electrical conductivity investigation

Electrical conductivity of BC and FNP-based WE was assessed under various experimental conditions to determine their performance and durability. Direct current

conductivity measurements were performed using a Keithley nanovoltmeter (2182A) paired with a current source (6221) at specific voltage and temperature settings. Electrical conductivity of the WE was evaluated after exposure to humidity for 8 h, at 40% relative humidity, in an atmosphere containing 0.2 % CO_2 at 40 ± 10 °C, using equipment from New Brunswick Instruments, Germany. Additionally, the WE was tested for changes in σDC under different temperatures (50 and 100 °C) in a vacuum oven (NSW India). The σDC measured at various temperatures was used to calculate activation energy (E_a) of BC and FNP using Arrhenius equation:

$$\sigma = \sigma o \exp(-Ea/kT) \quad (1)$$

where σ represents electrical conductivity, σo is pre-exponential factor, k is Boltzmann constant (1.38×10^{-22} J/K) and T is absolute temperature.

Results

FTIR analysis

BFS and BFN were characterized through FTIR spectral analysis to ascertain their formation, as evidenced by distinct characteristic wave numbers ($\bar{\upsilon}$, cm^{-1}) in Fig. 1. FTIR of BFS shows peaks at 650, 1064, 1381, 1632 and 3500 cm^{-1}, in which a prominent peak around 3500 cm^{-1} corresponds to ν_{O-H} stretching associated with hydrogen bonding, the one at 1740-1700 cm^{-1} reveals carbonyl-based surface functionalities and that at 1632 cm^{-1} shows presence of aromatic C=C and C=O stretching. An additional peak at 568 cm^{-1} corresponds to Sm-O vibration [35]. This clearly indicates introduction of Sm_2O_3 in FNP structure.

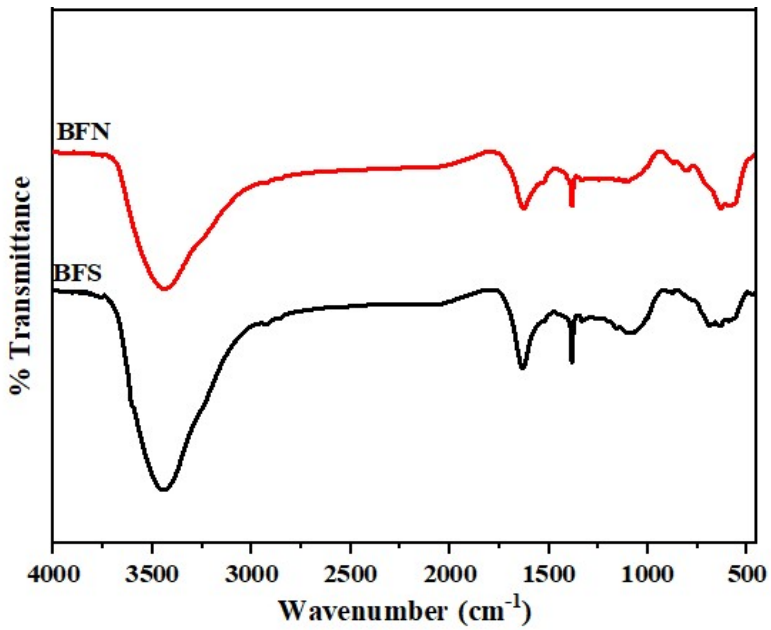

Figure 1: FTIR spectra of BFS and BFN.

Spectrum of BFN revealed the presence of peaks at 575, 632, 812, 877, 1064, 1381, 1632 and 3500 cm^{-1}. The small peaks at 575, 812 and 877 cm^{-1} are attributed to stretching vibrations of Nb-O [36]. This shows that Nb_2O_5 have been incorporated in structural framework of FNP.

UV-DRS analysis

UV-DRS analysis was utilized to determine λ_{max} and band gap energy of prepared NC by examining absorption edge in UV-Visible spectrum (Fig. 2).

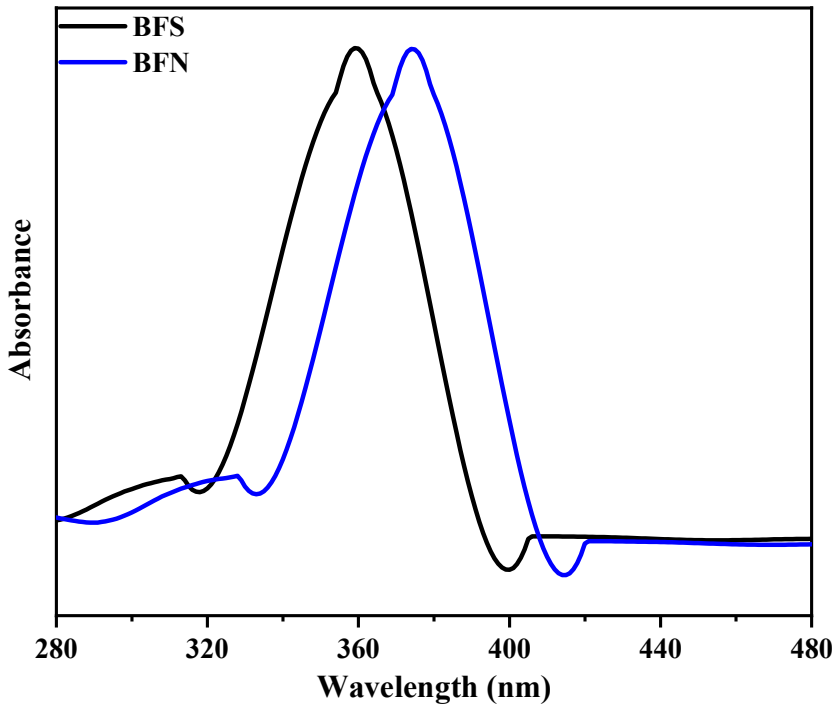

Figure 2: UV-DRS spectra of BFS and BFN.

The absorption band of BFS was observed at 358 nm. On the other hand, BFN exhibited a shift with an absorption band at 374 nm. BFS and BFN showed band gap energy value of 2.80 and 2.78 eV, respectively.

Microstructure analysis

SEM imaging of BFS and BFN derived WE were conducted at a standardized scale of 1 µm and 10 KX magnifications. SEM images of both WE depict agglomerated FNP grains dispersed over the flakes of BC along with amorphous phases of PVB. SEM microgram of BFS reveals uniform surface with Sm_2O_3 dispersed over BC matrix (Fig. 3a). On the other hand, BFN-incorporated WE exhibits uniformly distributed Nb_2O_5 and FNP over BC matrix (Fig. 3b).

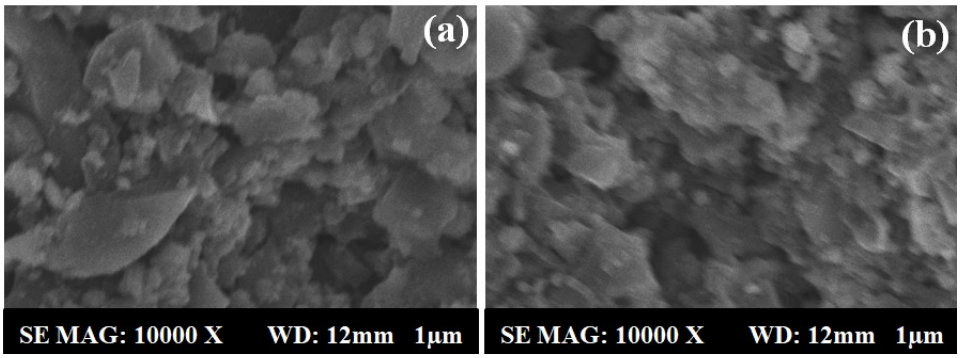

Figure 3: SEM micrographs of **(a)** BFS and **(b)** BFN at 10,000X magnification.

Thermal analysis

Thermogram of BFS reveals three step decomposition (Fig. 4a).

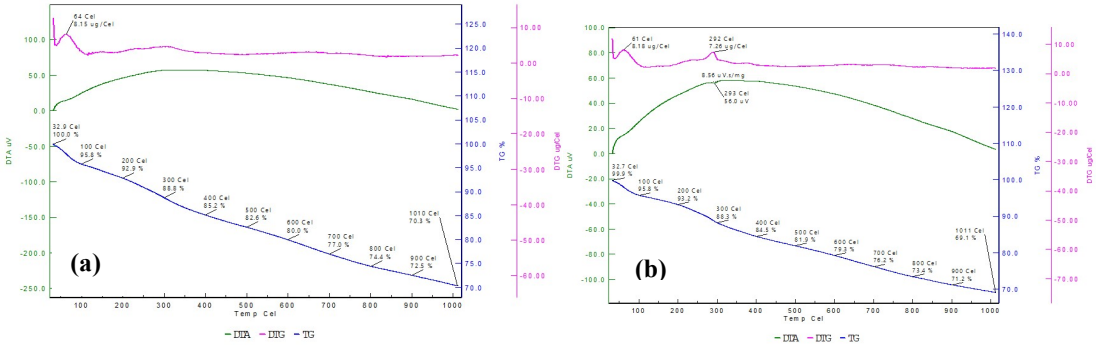

Figure 4: Simultaneous TG-DTA-DTG curves of **(a)** BC and **(b)** FNP.

BFS has rendered steep decomposition in the range from 32.7 to 100 ºC, leaving 95.8% Wr. Rapid decomposition appeared at 9.11 µg/ºC at 61 ºC in this narrow range. This was associated with an intense DTA signal of 11.72 µV, at 48 ºC. The 4.44 % weight loss in this range may result from volatilization of moisture content associated with BC. The second step commenced at TG_o of 100 ºC and TG_e of 300 ºC, leaving 88.34% Wr. The third step started at TG_o of 300 ºC and TG_e of 750 ºC, leaving 74.98% Wr. The 8.06 % weight loss in these regions may be due to degradation of residual initial substrate species like Sm_2O_3, BC and FNP. DTG revealed decomposition of 7.26 µg/ºC at 292 ºC, for this range. These steps were associated with an intense and broad DTA signal of 56 µV, at 293 ºC. Further increase in temperature from 750 to 1000 ºC rendered moderate decomposition of BFS at a rate of 3.10/ºC. Decomposition of BFS was terminated at 1000 ºC, leaving 69.1 weight% BC.

TGA of BFN revealed three step decomposition (Fig. 4b). First thermal decomposition step ranges from TG_o of 32.7 ºC to TGe of 100 ºC, leaving 95.8% W_r. In this step, rapid decomposition occurs at 9.11 µg/ºC, at 61 ºC. The 4.2% weight loss

in this narrow range may be ascribed to volatilization of moisture content associated with BFN. The second step was commenced at TG_o of 200 ºC and TG_e of 300 ºC leaving 88 % Wr. The 7.8 % weight loss in region may be attributed to the degradation of residual initial substrate species like Nb_2O_5, BC and FNP. DTG reveals decomposition at 7.26 µg/ºC at 292 ºC. Both of these steps are associated with a broad DTA signal of 56 µV at 293 ºC. Further increase in temperature from 500 to 1010 ºC rendered BFN slow decomposition at a rate of 2.20/ºC. Decomposition of BFN was concluded at 1011 ºC, leaving 69.1 weight% BC. Overall, both NC were found to be thermally stable upto 1010 ºC, leaving up to 70% Wr [37].

Electrical conductivity

Electrical conductivity of WE derived from BFS and BFN was thoroughly investigated to assess their operational performance and durability under various experimental conditions.

Current-voltage (I-V) characteristics of WE

I-V characteristics of WE were measured within the voltage range from 5 to 45 V. Analysis of electrical properties revealed that conductivity of BFN-derived WE exceeded that of BFS-based WE. Fig. 5 illustrates a linear increase in current with voltage for both BFS and BFN-derived WE, indicating ohmic conductive behavior in both materials and their ability to develop WE [33].

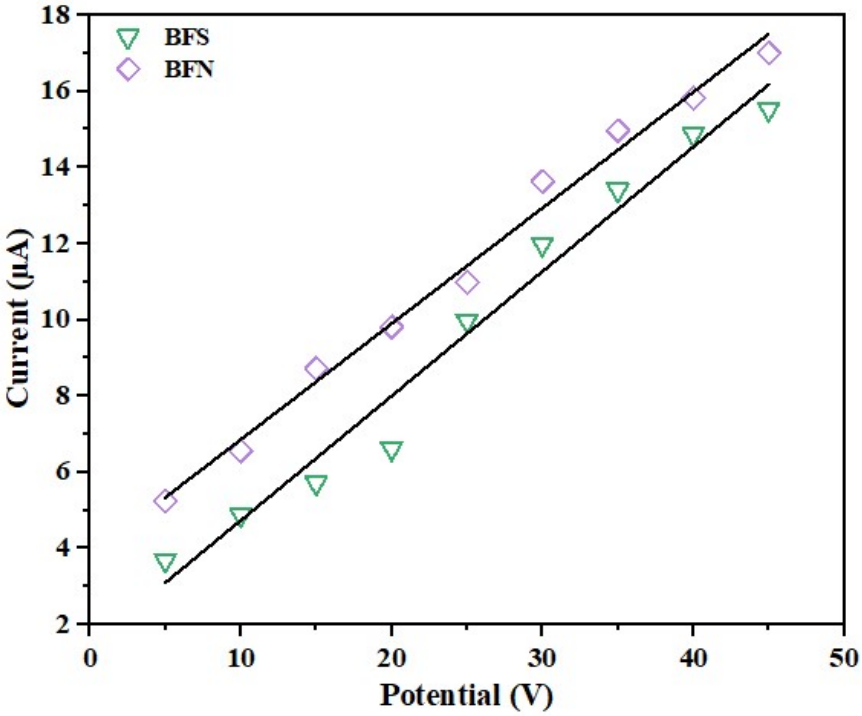

Figure 5: I-V curves of BFS and BFN-derived WE depicting Ohmic conductive behaviour.

Electrical conductivity at variable voltages

Electrical behavior of BFS and BFN was analyzed through their DC conductivity measurements at three different voltages (1, 10 and 100 V) at room temperature [1]. Results indicate that increasing voltage from 1 to 10 V did not significantly affect σDC. However, a marked increase in σDC was observed for both samples when voltage was raised from 10 to 100 V, with BFN exhibiting highest conductivity, reaching a peak value of 0.83 mS/cm (Fig. 6).

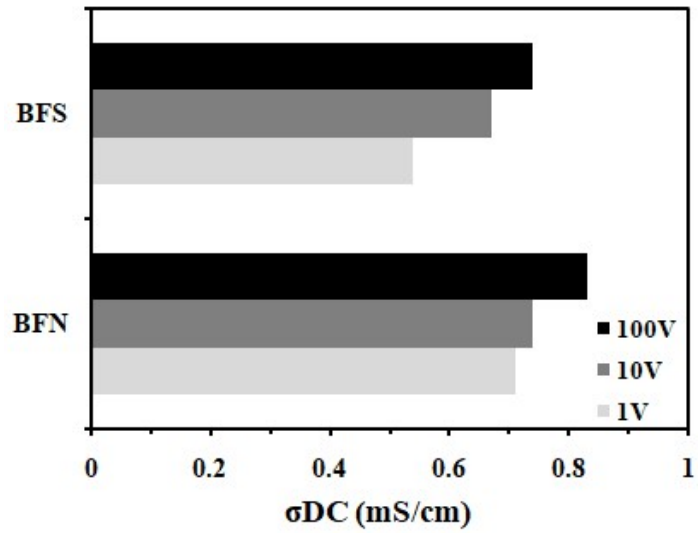

Figure 6: σDC of BFS and BFN-derived WE at 1, 10 and 100 V.

Results showcase superior electrical conductivity of BFN compared to BFS at all voltage levels, underlining BFN potential as an electrically conductive WE material. Improvement in electrical conductivity is likely due to reduction in the energy gap (Eg) following exfoliation of Nb and FNP over BC matrix [1]. These enhancements promote rapid electron transfer and result in higher σDC, making BFN a promising candidate for electrically conductive WE.

Temperature-dependent electrical conductivity analysis

Effect of temperature on σDC was studied over temperature range from 300 to 400 K, maintaining a constant voltage of 100 V. Activation energy was evaluated on both WE, for which purpose, Arrhenius plot was plotted between log(σDC) and 1000/T (K^{-1}) (Fig. 7).

BFS and BFN exhibited activation energy value of 27.64 and 26.36 J/mol, respectively. Results showcases that conductivity rises linearly with increase in temperature from 300 to 400 K. This analysis demonstrates that electrons exhibit lower activation energy for migration within conducting BFN than in the case of BFS-derived WE.

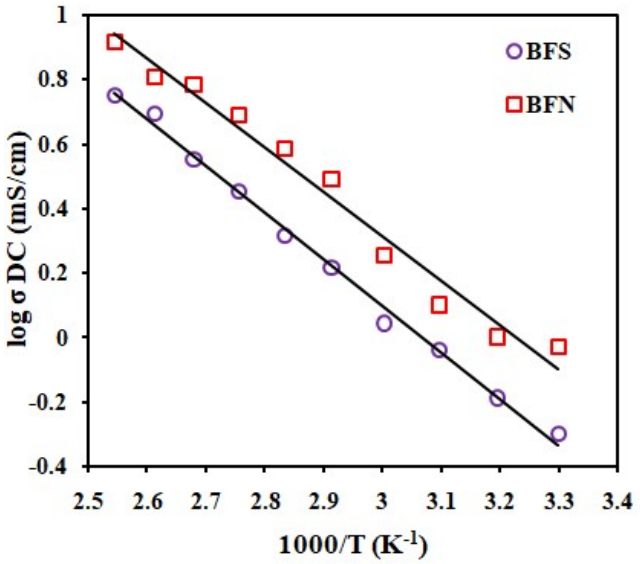

Figure 7: Arrhenius plot depicting effect of temperature on σDC of BFS and BFN.

Effect of humidity exposure on electrical conductance

Performance and durability of developed WE was also studied by observing their σDC after fixed time interval with exposure to the 4% humid environment (HE). Results illustrated in Fig. 8 depict variations in σDC as a function of HE exposure time over different WE. The WE were periodically assessed under HE at 1 h intervals for up to 8 h. WE developed from BFN and BFS exhibited a distinct pattern with progressive increase in σDC for 7 h of HE followed by a decrease (Fig. 8). BFN-coated WE showed higher electrical conductivity in comparison to BFS-coated WE throughout the experiment.

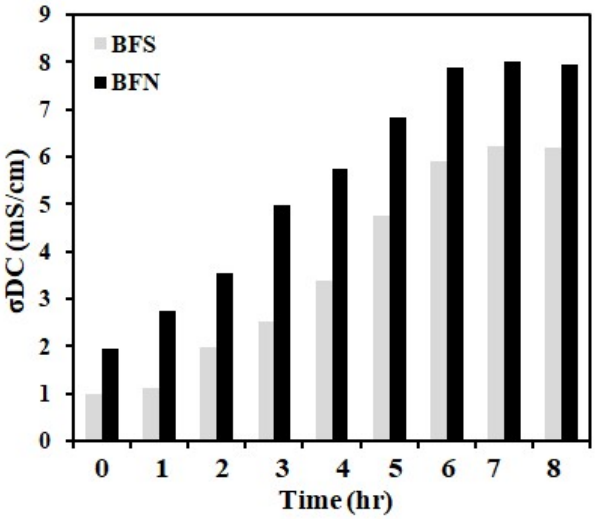

Figure 8: Effect of 40% relative humidity exposure on σ DC of BFS and BFN-derived WE for an 8 h period.

Baking effect on electrical performance

Effect of the heating process on the performance of developed WE was systematically examined, focusing on two specific temperature conditions: 50 and 100 °C, over a 12 h period. Results revealed that, at lower temperature of 50 °C, both WE exhibited a noticeable increase in their σDC values for 12 h of heating (Fig. 9(a)). In contrast, when subjected to a more elevated temperature of 100°C, WE displayed a different behavior. Here, σDC continued to rise over the initial 10 h of heating, followed by a reduction in conductivity (Fig. 9b).

This distinct trend suggests that the high-temperature environment may have induced a different set of degradation processes or structural transformations within the WE. In this case, the declining trend in σDC after an initial increase is indicative of potential adverse effects from prolonged exposure to elevated temperatures on the WE performance.

Decrease in σDC beyond 10 h is attributed to the WE having reached percolation threshold, after which conductivity values decline. This reduction in conductivity may result from prolonged exposure to harsh environmental conditions, leading to aggregation of metallic nanoparticles and consequent reduction on the number of free charge carriers.

Conversely, continuous increase in conductivity values indicates the stability of NC-based WE in humid and thermal environments without any significant dissociation of the prepared material. This stability underscores the suitability of developed NC as excellent electrically conductive materials for a wide range of applications.

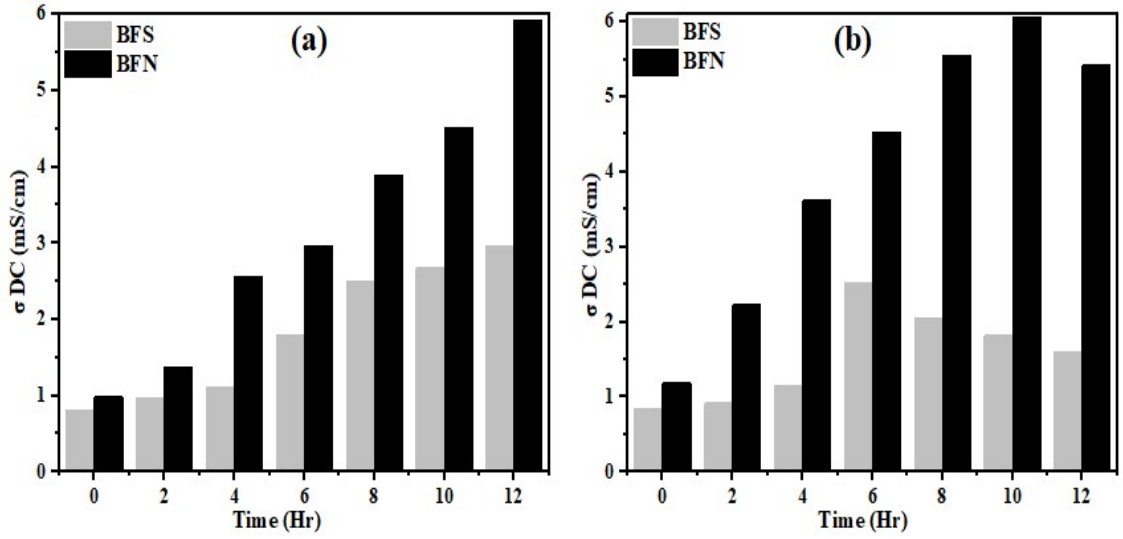

Figure 9: Effect of heating BFS and BFN derived-WE at **(a)** 50 °C and **(b)** 100 °C on their σDC.

Conclusion

In this study, Sm and Nb-doped BC/FNP NC was successfully synthesized. Comparative analysis was conducted for examining their electrical conductivity in different environmental conditions. Experimental findings demonstrate that Nb-doped NC exhibit superior DC conductivity (0.83 mS/cm) compared to their Sm-doped counterparts, irrespective of environmental conditions. This enhanced conductivity in Nb-doped NC can be attributed to efficient charge transport facilitated by electronic structure of Nb and its interaction with FNP matrix. UV-DRS analysis revealed band gap values of 2.80 and 2.78 for BFS and BFN, respectively. These results suggest that Nb doping is a more effective strategy for improving electrical properties of NC from BC/FNP, potentially expanding their application in electronic and energy storage devices. Further research could explore underlying mechanisms of this improvement, and evaluate long-term stability of these materials in practical applications.

Acknowledgement

This research work was supported by existing facilities Department of Chemistry, College of Basic Sciences and Humanities, G. B. Pant University of Agriculture and Technology, Pantnagar.

Conflict of interest

The authors declare no conflict of interest.

Authors' contributions

D. Palariya: resources; experimental work; data analysis; writing-review and editing. **M. Pandey and P. Joshi**: writing-review and editing. **J. Maheshwari**: editing; formal analysis. **S. Mehtab**: conceptualization; formal analysis; validation; review and editing; supervision. **M. G. H. Zaidi**: conceptualization; review and editing; supervision.

Abbreviations

BC: biochar composite
BFN: niobium doped Biochar/ferrite-based nanocomposites
BFS: samarium doped Biochar/ferrite-based nanocomposites
σDC: electrical conductivity
DTA: differential thermal analysis
DTG: derivative thermogravimetry,
FNP: ferrite nanoparticle
FTIR: Fourier tranform infrared spectroscopy
HE: humid environment
Nb_2O_5: niobium oxide

NC: nanocomposites
PVB: polyvinyl butyral
SEM: scanning electron microscopy
Sm_2O_3: samarium oxide
TG: thermogravimetry
Tge: thermogravimetry endset
Tgo: thermogravimetry onset
UV-DRS: ultraviolet-diffuse reflectance spectroscopy
WE: working electrodes
Wr: weight residue

References

1. Sharma S, Mehtab S, Zaidi MG. Effect of baking, humidity and UV radiation on hexagonal boron nitride modified c-MWCNT nanohybrid electrodes. Mater Tod Proc. 2022;62(12):6494-7. https://doi.org/10.1016/j.matpr.2022.04.234
2. Panahi HK, Dehhaghi M, Ok YS et al. A comprehensive review of engineered biochar: production, characteristics and environmental applications. J Clean Prod. 2020;270:122462. https://doi.org/10.1016/j.jclepro.2020.122462
3. Niu Z, Feng W, Huang H et al. Green synthesis of a novel Mn–Zn ferrite/biochar composite from waste batteries and pine sawdust for Pb^{2+} removal. Chemosphere. 2020;252:126529. https://doi.org/10.1016/j.chemosphere.2020.126529
4. Du C, Song Y, Shi S et al. Preparation and characterization of a novel Fe_3O_4-graphene-biochar composite for crystal violet adsorption. Sci Tot Environ. 2020;711:134662. https://doi.org/10.1016/j.scitotenv.2019.134662
5. Zhang P, O'Connor D, Wang Y et al. A green biochar/iron oxide composite for methylene blue removal. J Haz Mater. 2020;384:121286. https://doi.org/10.1016/j.jhazmat.2019.121286
6. Chen M, Tao X, Wang D et al. Facilitated transport of cadmium by biochar-Fe_3O_4 nanocomposites in water-saturated natural soils. Sci Tot Environ. 2019;684:265-75. https://doi.org/10.1016/j.scitotenv.2019.05.326
7. Jung KW, Choi BH, Jeong TU et al. Facile synthesis of magnetic biochar/Fe_3O_4 nanocomposites using electro-magnetization technique and its application on the removal of acid orange 7 from aqueous media. Bioresour Technol. 2016;220:672-6. https://doi.org/10.1016/j.biortech.2016.09.035
8. Sun P, Hui C, Azim Khan R et al. Efficient removal of crystal violet using Fe_3O_4-coated biochar: the role of the Fe_3O_4 nanoparticles and modeling study their adsorption behavior. Sci Rep. 2015;5(1):12638. https://doi.org/10.1038/srep12638

9. Jung KW, Lee SY, Lee YJ. Facile one-pot hydrothermal synthesis of cubic spinel-type manganese ferrite/biochar composites for environmental remediation of heavy metals from aqueous solutions. Bioresour Technol. 2018;261:1-9. https://doi.org/10.1016/j.biortech.2018.04.003
10. Podder MS, Majumder CB. SD/$MnFe_2O_4$ composite, a biosorbent for As (III) and As (V) removal from wastewater: Optimization and isotherm study. J Mol Liq. 2015;212:382-404. https://doi.org/10.1016/j.molliq.2015.09.011
11. Nalbandian L, Patrikiadou E, Zaspalis V et al. Magnetic nanoparticles in medical diagnostic applications: synthesis, characterization and proteins conjugation. Curr Nanosci. 2016;12(4):455-68. https://doi.org/10.2174/1573413712666151210230002
12. Bakr AS, Moustafa YM, Motawea EA et al. Removal of ferrous ions from their aqueous solutions onto $NiFe_2O_4$–alginate composite beads. J Environ Chem Eng. 2015;3(3):1486-96. https://doi.org/10.1016/j.jece.2015.05.020
13. Xavier JR. Retracted: Synthesis and characterization of polypyrrole/graphitic carbon nitride/niobium pentoxide nanocomposite for high-performance energy storage applications. J Appl Polym Sci. 2024;141(15):e55211. https://doi.org/10.1002/app.55211
14. Hamzad S, Kumar KY, Prashanth MK et al. Boron doped RGO from discharged dry cells decorated Niobium pentoxide for enhanced visible light-induced hydrogen evolution and water decontamination. Surf Interf. 2023;36:102544. https://doi.org/10.1016/j.surfin.2022.102544
15. Huang H, Zhou J, Zhou J et al. Structure-retentive synthesis of a highly ordered mesoporous Nb_2O_5/N-doped graphene nanocomposite with superior interfacial contacts and improved visible-light photocatalysis. Catal Sci Technol. 2019;9(13):3373-9. https://doi.org/10.1039/C9CY00555B
16. Ghouri MI, Ahmed E, Ali A et al. Improved photocatalytic H_2 evolution over composites based on niobium pentoxide, metal sulfides and graphene. Mater Sci Semicond Proc. 2021;122:105492. https://doi.org/10.1016/j.mssp.2020.105492
17. Ramesan MT, Sampreeth T. Synthesis, characterization, material properties and sensor application study of polyaniline/niobium doped titanium dioxide nanocomposites. J Mater Sci Mater Electron. 2017;28:16181-91. https://doi.org/10.1007/s10854-017-7519-9
18. Qamar M, Abdalwadoud M, Ahmed MI et al. Single-pot synthesis of ⟨001⟩-faceted N-doped Nb_2O_5/reduced graphene oxide nanocomposite for efficient photoelectrochemical water splitting. ACS Appl Mater Interf. 2015;7(32):17954-62. https://doi.org/10.1007/10.1021/acsami.5b04667

19. Chennakesavulu K, Reddy GR, Prasath SS et al. Visible light driven photocatalytic degradation of the reactive red-198, methylene blue and 3-chlorophenol by Nb_2O_5@ ZnO: Synthesis and characterization. Adv Mater Lett. 2015;6:518-26. http://dx.doi.org/10.5185/amlett.2015.5776
20. Rafael RA, Noronha FB, Gaspar AB. Synthesis and Characterization of Ti-Nb_2O_5 Catalysts for Discoloration Reaction of Bromophenol Blue and Indigo Carmine Dyes. Top Catal. 2020;63:1066-76. https://doi.org/10.1007/s11244-020-01313-z
21. Lazar NE, Mazkad D, Moussadik A et al. High-performance ferroelectric photocatalysts for rapid dye degradation: ZrO_2-doped $LiTa_0.5Nb_0.5O_3$ under solar UV light. J Sol-Gel Sci Technol. 2024;110(1):233-45. https://doi.org/10.1007/s10971-024-06330-y
22. Kozlovskiy A, Egizbek K, Zdorovets MV et al. Evaluation of the efficiency of detection and capture of manganese in aqueous solutions of FeCeOx nanocomposites doped with Nb_2O_5. Sensors. 2020;20(17):4851. https://doi.org/10.3390/s20174851
23. Mahalakshmi G, Ponnarasi P, Rajeswari M. A eco-friendly, low cost green synthesis of Ag@Sm_2O_3/rGO nanocomposites with enhanced UV light photocatalytic and antimicrobial activity. Inorg Chem Commun. 2024;161:111811. https://doi.org/10.1016/j.inoche.2023.111811
24. Jamnani SR, Moghaddam HM, Leonardi SG et al. PANI/Sm_2O_3 nanocomposite sensor for fast hydrogen detection at room temperature. Synth Met. 2020;268:116493. https://doi.org/10.1016/j.synthmet.2020.116493
25. El Maati LA, Khosa RY, Alahmari SD et al. Facile synthesis of environmental friendly Sm_2O_3/rGO electrode as an alternative source for energy storage devices. Diam Relat Mater. 2024;142:110769. https://doi.org/10.1016/j.diamond.2023.110769
26. Wassel AR, Abdelhameed RM, Nasralla NH et al. Impact of Sm_2O_3 onthe morphological, optical, magnetic and pesticide adsorption of Co_3O_4/PANI hybrid nanocomposites. ECS J. Sol Stat Sci Technol. 2022;11(8):083009. https://doi.org/10.1149/2162-8777/ac84a6
27. Khan MM, Matussin SN. Sm_2O_3 and Sm_2O_3-based nanostructures for photocatalysis, sensors, CO conversion and biological applications. Catal Sci Technol. 2023;13(8):2274-90. https://doi.org/10.1039/D2CY01976K
28. Palariya D, Mehtab S, Aziz M et al. Exploring rare earth element doped nanocomposites as promising photocatalysts for dyes degradation in water. Wat Air Soil Pollut. 2024;235(5):286. https://doi.org/10.1007/s11270-024-07076-7

29. Muneer I, Farrukh MA, Javaid S et al. Synthesis of Gd_2O_3/Sm_2O_3 nanocomposite via sonication and hydrothermal methods and its optical properties. Superlattices Microstruct. 2015;77:256-66. https://doi.org/10.1016/j.spmi.2014.10.006
30. Alshammari MH, Alshammari AO, Elabbasy MT et al. Surface morphology and cell viability of samarium (III) oxide/chromium (III) oxide/graphene oxide/polycaprolactone targeting wound dressing. J Rare Earths. 2024;42(3):555-561. https://doi.org/10.1016/j.jre.2023.04.010
31. Javaid, A and Farrukh, MA. Comparison of photocatalytic and antibacterial activities of allotropes of graphene doped Sm_2O_3 nanocomposites: Optical, thermal and structural studies. J Chin Chem Soc. 2023;70(1):32-45. https://doi.org/10.1002/jccs.202200478
32. Dezfuli AS, Ganjali MR, Naderi HR. Anchoring samarium oxide nanoparticles on reduced graphene oxide for high-performance supercapacitor. Appl Surf Sci. 2017;402:245-53. https://doi.org/10.1016/j.apsusc.2017.01.021
33. Mehtab S, Zaidi MG, Singh A et al. Electrochemical monitoring of congo red degradation using strontium titanate-doped biochar nanohybrids derived photocatalytic plates. Environ Sci Pollut Res. 2025;32(12):7181-93. https://doi.org/10.1007/s11356-023-28633-3
34. Maheshwari J, Palariya D, Bughani A et al. Biochar supported metal oxide nanocomposites for electrochemical estimation of simazine in water samples. Chem Pap. 2025;2:1-7. https://doi.org/10.1007/s11696-025-03964-2
35. Putri N, Yulizar Y, Umar A, Apriandanu DO. Sm_2O_3 nanoparticles preparation using caesalpinia pulcherrima leaf extract, characterization and photocatalytic activity. In IOP Conference Series: Mater Sci Eng. 2020;902(1):012012. IOP Publishing. https://doi.org/10.1088/1757-899X/902/1/012012
36. Reddy LB, Prakash HR, Ravikiran YT et al. Structural and humidity sensing properties of niobium pentoxide-mixed nickel ferrite prepared by mechano-chemical mixing method. J Mater Sci Mater Electron. 2020;31:21981-99. https://doi.org/10.1007/s10854-020-04701-z
37. Pandey M, Joshi P, Mehtab S et al. Thermal degradation and kinetic analysis of fly ash-enriched epoxy composites. Bulg Chem Commun. 2023;55(A):71-76. https://doi.org/10.34049/bcc.55.A.0011